

Design and Analysis of Low-Voltage Current-Mode Logic Buffers

Payam Heydari

Department of Electrical and Computer Engineering
University of California, Irvine
Irvine, CA 92697-2625

Abstract - This paper investigates important problems involved in the design of a CML buffer as well as a chain of tapered CML buffers. A new design procedure to systematically design a chain of tapered CML buffers is proposed. The differential architecture of a CML buffer makes it functionally robust in the presence of environmental noise sources (e.g., crosstalk, power/ground noise). The circuit design issues in regard to the CML buffer are compared with those in a conventional CMOS inverter. It is shown, both through the experiments and by using efficient analytical models, why CML buffers are better than CMOS inverters in high-speed low-voltage applications.

1. INTRODUCTION

Static CMOS logic style is commonly used in the design of digital integrated circuits due to its advantages such as very low static-power dissipation, high packing density and wide noise-margins. However, this logic family is highly susceptible to environmental noise sources such as electromagnetic coupling, power/ground noise, and substrate noise; and its maximum operating frequency is orders of magnitudes less than f_T of the MOS device. It also suffers from a large dynamic power dissipation at high-frequencies.

Designing a high-speed CMOS circuit operating near f_T of the MOS device is very challenging. System blocks in a giga-bit communication system need to be realized by very simple circuits utilizing minimum number of active devices. Parts of the circuit blocks that process high-speed signals in a communication transceiver should possibly abandon to use PMOS devices due to their inferior unity-gain frequency. On the other hand, Buffers are the circuit core of many high-speed blocks within a communication transceiver and a serial link. Front-end tapered buffer chain, serial-to-parallel converters, clock and data recovery (CDR), multiplexers, and demultiplexers all use high-speed buffers with a robust performance in the presence of noise. The electromagnetic coupling causes serious operational malfunctioning in the circuits particularly single-ended circuits. [1] [2].

CMOS current-mode logic buffers were first introduced in [3] to implement a giga-hertz MOS adaptive pipeline technique. the CML circuits can operate with lower signal voltage and higher operating frequency at lower supply voltage than CMOS circuits can. However, CML buffers suffer from dissipating more static power than CMOS inverters. Recently, there have been efforts to alleviate this shortcoming [4]. Due to their superior performance, CML buffers are the best choice for high-speed applications. As a consequence, it is an essential need to have a systematic approach to optimally design CML buffers and CML buffer chains.

This paper presents a comprehensive study of CML buffers and steps that need to be taken to design a chain of tapered CML buffer. The paper is organized as follows. First, in section 2, the large-signal behavior of a differential circuit is extensively illustrated. This will prepare us to study the design of CMOS buffer chain (section 3). Finally, section 4 provides the experimental results that verify the accuracy of our design approach.

2. CURRENT-MODE LOGIC BUFFERS

A current-mode logic (CML) buffer is based on the differential architecture. Fig. 1. (a) shows a basic differential architecture. The tail current, I_{SS} , provides an input-independent biasing for the circuit. The differential circuit is easily neutralized using a pair of capacitors (Fig. 1.(a)), C_D , that will diminish the deleterious effects of input-output coupling through the device overlap capacitance, C_{GD} .

Various experimental simulations of CML circuits reveal that the long-channel transistor model still gives rise to a good estimation of the dynamic behavior of these circuits. The reason is because a CML circuit is a low-voltage circuit where the differential voltage swing is around the device threshold voltage.

As the differential input varies from $-\infty$ to $+\infty$, each output node of the differential pair varies from $V_{DD} - R_D I_{SS}$ to V_{DD} . Fig. 1 (b) shows the voltage variations of the output nodes in terms of the differential input [5].

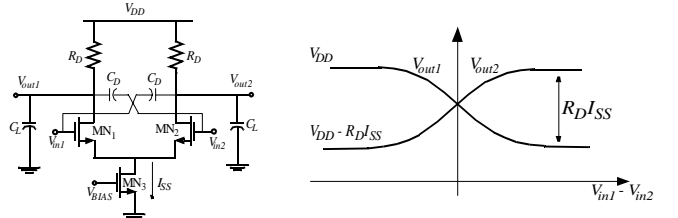


Fig. 1. (a) A neutralized CMOS differential pair. (b) Transfer characteristics.

From Fig. 1. (a) one can see that the maximum output differential voltage swing, V_{odm} , is only a function of the drain resistor and the tail current, provided that the current switching takes place. Clearly, the maximum output swing of a CML buffer is less than that of a CMOS inverter, which makes this class of buffers an ideal choice for low-power integrated circuit design.

The minimum value of the input common-mode level, $V_{in,CM,min}$, is achieved when the tail current begins to operate in saturation. The input common-mode level reaches its maximum value, $V_{in,CM,max}$, when the transistors MN_1 and MN_2 are either at pinch-off or at cutoff [5].

$$V_{GS,12} + (V_{GS3} + V_{THN}) \leq V_{in,CM} \leq \min \left[V_{DD} - R_D \frac{I_{SS}}{2} + V_{THN}, V_{DD} \right] \quad (1)$$

where V_{GS12} is the common-mode overdrive voltage of transistors MN_1 and MN_2 . Similarly, the output common-mode level varies from V_{DD} (when both MN_1 and MN_2 are off, and MN_3 is in the linear region) to $V_{DD} - R_D I_{SS}/2$ (when all transistors are in saturation). The voltage transition of the output common-mode level from V_{DD} to $V_{DD} - R_D I_{SS}/2$ is determined by the subthreshold current of MN_1 or MN_2 .

The advantage of the differential CML buffer is understood by reviewing its large-signal behavior in response to a differential

input signal. Assuming that the input common-mode level is bounded within the operating range specified in Eq. (1), a small voltage difference between V_{in1} and V_{in2} results in a corresponding differential current $I_{D1}-I_{D2}$, as follows [5]:

$$\Delta I_D = I_{D1} - I_{D2} = \frac{1}{2} \mu_n C_{ox} \frac{W}{L} \Delta V_{in} \sqrt{\frac{4I_{SS}}{\mu_n C_{ox} \frac{W}{L}} - \Delta V_{in}^2} \quad (2)$$

The differential current is an odd function of the input differential voltage, ΔV_{in} , and thus becomes zero when the circuit is in equilibrium. Furthermore, a differential stage is more linear than a single-ended stage due to the absence of the even harmonics from the input-output characteristics. The large-signal transconductance, G_m , is the slope of $\Delta I_D - \Delta V_{in}$ transfer characteristics, that is:

$$G_m = \frac{1}{2} \mu_n C_{ox} \frac{W}{L} \frac{2\Delta V_{in,max}^2 - 2\Delta V_{in}^2}{\sqrt{2\Delta V_{in,max}^2 - \Delta V_{in}^2}} \quad (3)$$

where $\Delta V_{in,max} = \sqrt{2I_{SS}/(\mu_n C_{ox} \frac{W}{L})}$. The large-signal transconductance varies with the input differential voltage, as also shown in Fig. 2, where in this figure $\Delta V_{in,max} = 0.4$ V. As the input differential voltage exceeds a limit, one transistor carries the entire current, I_{SS} , turning off the other transistor. $\Delta V_{in,max}$ represents the maximum input differential voltage.

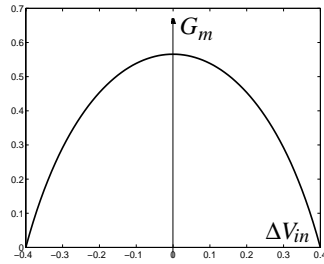


Fig. 2. Large-signal G_m as a function of the differential input

An input-dependent transconductance results in a nonlinear large-signal gain. To simplify the analysis the average value of the transconductance is utilized.

$$G_{m,avg} = \frac{\int_0^{\Delta V_{in,max}} G_m(\Delta V_{in}) d(\Delta V_{in})}{\int_0^{\Delta V_{in,max}} d(\Delta V_{in})} = \sqrt{\frac{1}{2} \mu_n C_{ox} \frac{W}{L} I_{SS}} \quad (4)$$

A differential pair architecture using a differential signaling is insensitive to common-mode fluctuations, which makes it a better choice as a buffer than a CMOS inverter, particularly in low-noise circuit design where noise mostly appears as a common-mode component. Moreover, a non-inverting buffer is easily realized using a single differential stage, as opposed to the CMOS inverter where a non-inverting buffer is realized by two inverters in cascade. Therefore, a non-inverting differential buffer exhibits a lower propagation delay than a CMOS buffer. A differential stage will be operating as a CML buffer iff a complete current switching takes place. To make sure that the current switches entirely from one side of the differential stage to the other side, the differential input voltage must be at least $\Delta V_{in,max}$.

Moreover, a differential CML buffer exhibits a higher bandwidth than a conventional CMOS inverter. This is readily proved either using the time-domain delay analysis or small-signal approximation.

3. TAPERED CML BUFFER DESIGN

To achieve the best performance in a CML buffer, a complete current switching must take place, and the current produced by the

tail current needs to flow through the ON branch only. In a tapered buffer chain a CML buffer drives another buffer, which means that output terminals of the driving buffer stage are connected to the input terminals of the driven stage, as shown in Fig. 3. To satisfy the above performance requirement, the differential voltage swing of the first CML buffer must exceed $\Delta V_{in2,max}$ of the following stage:

$$R_{D1} I_{SS1} \geq \sqrt{2I_{SS2} / \left(\mu_n C_{ox} \left(\frac{W}{L} \right)_2 \right)} \quad (5)$$

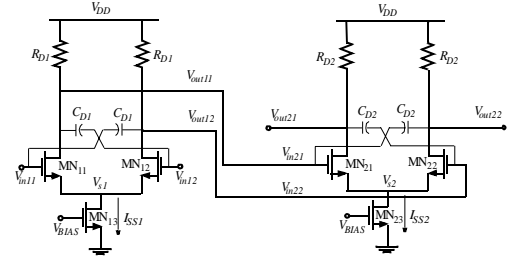


Fig. 3. Two CML buffers in cascade

Furthermore, the load resistors should be small in order to reduce the RC delay and increase the bandwidth. To guarantee a high-speed operation, NMOS transistors of the differential pair must operate only in the saturation. To satisfy this requirement for the circuit shown in Fig. 3, first, the input common-mode voltage must be within the interval specified in Eq. (1); and secondly,

$$V_{in,k,max} - V_{THN} \leq V_{out,kj} \leq V_{DD} \quad \text{for } k = 1, 2 \text{ and } j = 1, 2 \quad (6)$$

which sets a maximum allowable level for the differential output swing as follows:

$$R_{Dk} I_{SSk} \leq V_{THN} \quad \text{for } k = 1, 2 \quad (7)$$

In addition, a high-speed CML output driver must drive a large off-chip load through the bondwire and package trace. The output driver must thus have a large current drive capability. This means that NMOS transistors of the second CML buffer in Fig. 3 must be large. A large transistor has a large gate-to-channel capacitance that seriously degrades the propagation delay and the voltage swing of the preceding predriver stage. To reduce the propagation delay of the predriver, a chain of tapered buffers is introduced between the first predriver stage and the second buffer. The minimum delay is obtained by dividing the delay equally over all stages. This is achieved by gradually scaling up all stages with a constant taper factor, u . On the other hand, the chip package interface at very high frequencies is appropriately modeled as a transmission line that is terminated by a load impedance, which is a series RC circuit (*cf.* Fig. 4). The series load resistance, Z_0 , provides the high-frequency parallel matched termination to the bondwire. Fig. 4 shows the schematic of the output CML driver driven by $N-1$ tapered CML buffers along with the chip-package interface being modeled as the transmission line.

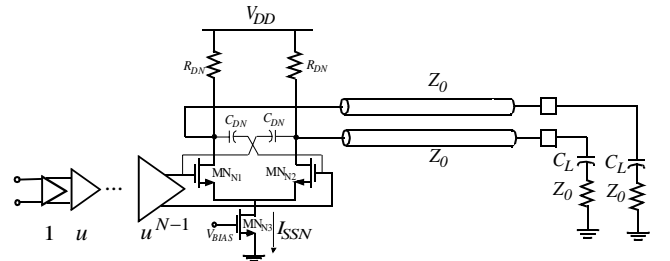


Fig. 4. An output CML buffer driving off-chip loads. The chip-package interface is electrically modeled using a lossless transmission line.

The chip bondwires exhibit high-Q inductances. Therefore it is safe to model the chip-package interface using a lossless transmission line. To avoid potentially disastrous transmission line effects such as slow ringing and propagation delays, the bondwires are terminated both at the source using a series termination ($R_{DN} = Z_0$), and at the destination using a parallel termination (Z_0). Given a well-defined output voltage swing ($R_D I_{SS}$) and with R_D being determined by the matched termination, the tail current I_{SSN} is easily calculated. For instance, an output differential voltage swing of 0.4V for a 50Ω line driver requires a bias current of 8mA. Now, using a set of constraints, we present design guidelines to design a tapered CML buffer chain and determine appropriate values for the circuit components of the CML buffer.

The propagation delay is computed using the open-circuit time constant method [6]. For instance, the delay of the simple low-voltage differential stage of Fig. 1 (a) is $0.69 R_D C_L$. Various HSPICE simulations on high-speed CML buffers show that the delay obtained by the open-circuit time-constant method is within 8% of the actual simulation.

Minimizing the overall propagation delay of CML buffer increases the overall operation frequency of the buffer significantly. For a slowly varying input signal, increasing the small-signal voltage gain will further decrease the output transient variations and the output transition time. In a chain of tapered CML buffers, to attain a constant voltage swing, transistor sizes are scaled up while the drain resistances are scaled down with a constant scaling factor. This will lead us to the fact that small-signal voltage gains of all constituting stages of the buffer chain are identical.

$$\sqrt{\mu_n C_{ox} \left(\frac{W}{L}\right)_1 I_{SS1} R_{D1}} = \sqrt{\mu_n C_{ox} \left(\frac{W}{L}\right)_2 I_{SS2} R_{D2}} = \dots = \sqrt{\mu_n C_{ox} \frac{W}{L} I_{SS} R_D}$$

As a consequence, Eq. (5) provides us with a lower bound for the maximum small-signal voltage gain at equilibrium, that is:

$$\left(A_{v,eq} = \sqrt{\mu_n C_{ox} \frac{W}{L} I_{SS} R_D}\right) \geq \sqrt{2} \quad (8)$$

The drain resistor, R_{DN} , of the last output CML buffer is determined by the series impedance matching to bondwire's characteristic impedance. Subsequently, I_{SSN} of the last driver stage is calculated using the output differential voltage swing and R_D . The only remaining parameter in the last CML driver left is the (W/L) of the source-coupled transistor pair, which is obtained from the common-mode characteristic of the last CML buffer. If the common-mode input voltage lies in the allowable range given by Eq. (1), then the tail current is equally divided between the two branches of the differential stage, i.e.,

$$(V_{in_k,CM} - V_{sk} - V_{THN} \geq V_{in_k,CM} - V_{BIAS} - 2V_{THN}) = \sqrt{I_{SSk} / \left(\mu_n C_{ox} \left(\frac{W}{L}\right)_k\right)} \quad (9)$$

for $k = 1, 2, \dots, N$

where $V_{in_k,CM}$ is the common-mode input voltage of the k^{th} driver in the buffer chain. $V_{in_k,CM}$ is specified by the output common-mode voltage of the previous stage. Given a **tapered buffer chain** with a constant differential voltage swing, the maximum (W/L) of the transistor pair of the k^{th} CML buffer is then calculated by solving Eq. (10):

$$V_{DD} - R_D \frac{I_{SS}}{2} - V_{BIAS} - 2V_{THN} = \sqrt{I_{SSk} / \left(\mu_n C_{ox} \left(\frac{W}{L}\right)_k\right)} \quad (10)$$

In the above equation $R_D I_{SS}$ is the constant differential output swing of a tapered CML buffer chain.

As mentioned above, in a chain of tapered CML buffers, the minimum delay is obtained by dividing the delay equally over all stages. However, the question is how many buffer stages are required to achieve the optimum delay. To answer this question, the propagation delay of an arbitrarily chosen CML stage in a buffer chain is first derived. Fig. 5 shows the k^{th} stage in a chain of N tapered stages driving another CML stage along with the capacitors that contribute to the delay calculation.

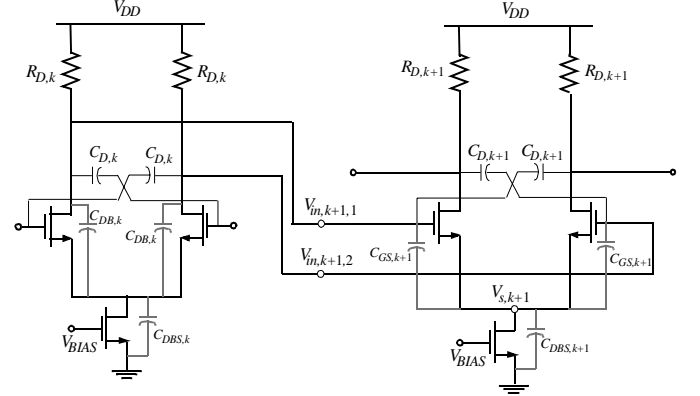


Fig. 5. The k^{th} and $(k+1)^{\text{st}}$ stages of a tapered CML buffer along with the parasitic capacitances

The common node s_{k+1} shown in Fig. 5 undergoes a smaller variation compared to the voltage variations of the input terminals particularly in a matched differential pair. In fact, it is easily shown that for a maximum differential input variation of $\Delta V_{in,max}$ derived in Section 2, the maximum variation of the common node is $\Delta V_{in,max} / \sqrt{2}$. Therefore, the equivalent capacitance seen at the common node s_{k+1} is approximately $C_{s,k+1} = \sqrt{2} C_{DBS,k+1}$ rather than $C_{DBS,k+1}$.

The 50% delay of the k^{th} stage is as follows:

$$t_{d,k} = 0.69 R_{D,k} (C_{DB,k} \otimes C_{s,k} + C_{GS,k+1} \otimes C_{s,k+1}) \quad (11)$$

where \otimes represents the series connection of electrical elements. The total propagation delay of the buffer chain is readily calculated:

$$t_d = \sum_{k=1}^N t_{d,k} = 0.69 N R_{D1} (C_{DB1} \otimes C_{s1} + X^{1/N} C_{GS1} \otimes C_{s1}) \quad (12)$$

Interestingly, the functional dependence between delay and the number of stages (or taper factor) is similar to the one in a CMOS buffer chain [7]. To be more specific, consider a chain of tapered CML buffers driving a lossless transmission line with a characteristic impedance of Z_0 . Suppose that the gate aspect-ratio of the transistor pair of the last CML line driver is X times larger than that of the first predriver stage. It is easily proved that if $C_{DB1} = \gamma C_{s1}$ and $C_{GS1} = \eta C_{s1}$; then it is easily proved that the optimum number of stages will be the numerical solution to the following equation:

$$X^{1/N_{opt}} = \exp \left[\frac{\frac{\gamma/\eta}{1+\gamma} + \left(\frac{1}{1+\eta}\right) X^{1/N_{opt}}}{\left(\frac{1}{1+\eta}\right) X^{1/N_{opt}}} \right] \quad (13)$$

or in the special case, if $C_{DB1} \ll C_{GS1}$ then, $N_{opt} = \ln(X)$ which is well-known result.

To further increase the bandwidth (reduce the delay), the intermediate stages use inductive peaking as demonstrated in Fig. 6.

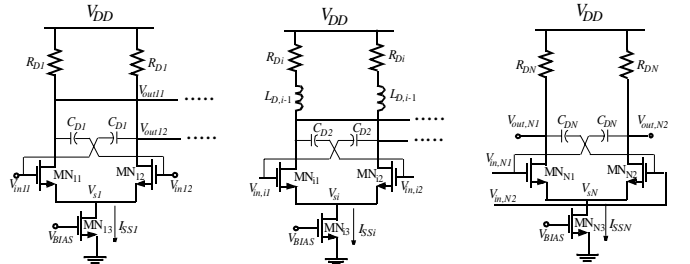


Fig. 6. Multiple stage CML buffers along with the inductive peaking

The addition of the inductor in series with the drain resistor delays the current flow through the branch containing the resistor, making more current available for charging the device capacitors, and reducing the rise and fall times. From another perspective, the addition of an inductance in series with the load capacitance introduces a zero in the transfer function of the CML stage which helps offset the roll-off due to parasitic capacitances. Inductive peaking can increase the bandwidth to about 1.72 times larger than the unpeaked case [6]. Inductance values are scaled with the same taper factor as the drain resistors are.

4. EXPERIMENTAL RESULTS

In this section the performance of the CML buffer is evaluated by performing experiments on single stage as well as multiple stages of the buffer. First, the noise susceptibility of the CML buffer is experimentally compared with CMOS inverter. Next, the accuracy of Eq. (13) is verified by running HSPICE simulation on a chain of CML buffers. Finally, the effect of inductive peaking on the bandwidth and speed enhancement will be investigated.

4.1. Noise Performance

A CML buffer exhibits a superior noise performance compared to a conventional CMOS inverter, particularly because environmental noise sources (e.g., crosstalk, power/ground noise) appear as common-mode signals. This will be experimentally verified by performing the following experiment.

First, crosstalk noise is emulated using parallel interconnects located within close proximity of each other, as depicted in figures 7 (a) and (b).

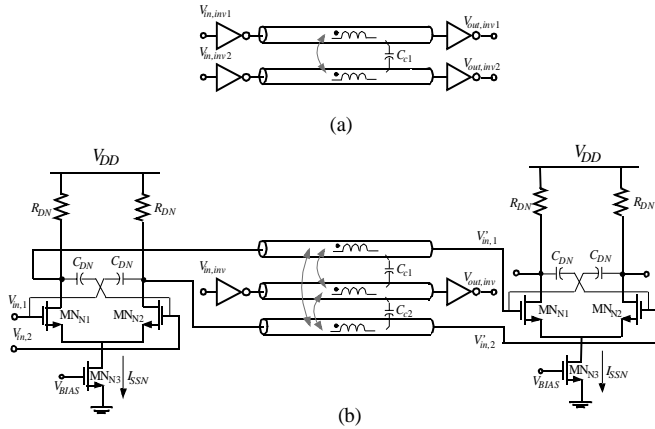


Fig. 7. (a) CMOS inverters driving two adjacent coupled interconnects that are terminated by CMOS inverters. (b) Two interconnects driven by a CML buffer and coupled to another interconnect which is driven by CMOS inverter.

To have a performance comparison, we place, first, a CMOS inverter, and then, a CML buffer at the outputs of coupled interconnects, one at a time (figures 7 (a) and (b)). To highlight the superiority of noise performance of the CML buffer, the middle line in Fig. 7 (b) will be driven by a CMOS inverter. The noise amplitude coupled from this line to its neighboring lines is, therefore, excessively large. The input signal frequency for all CMOS inverters is 3.3GHz, while it is 3.5GHz for CML buffers. As a consequence, this experiment also shows the performance of CML buffer in the presence of harmonic distortion. All circuits are designed using 0.18 μ m standard MOS process.

Figures 8 (a) and (b) demonstrate the output signals of CMOS inverter and CML buffer, respectively. The experiment is set up to demonstrate the worst-case scenario in which the noise fluctuation and the voltage waveform are 80° out of phase.

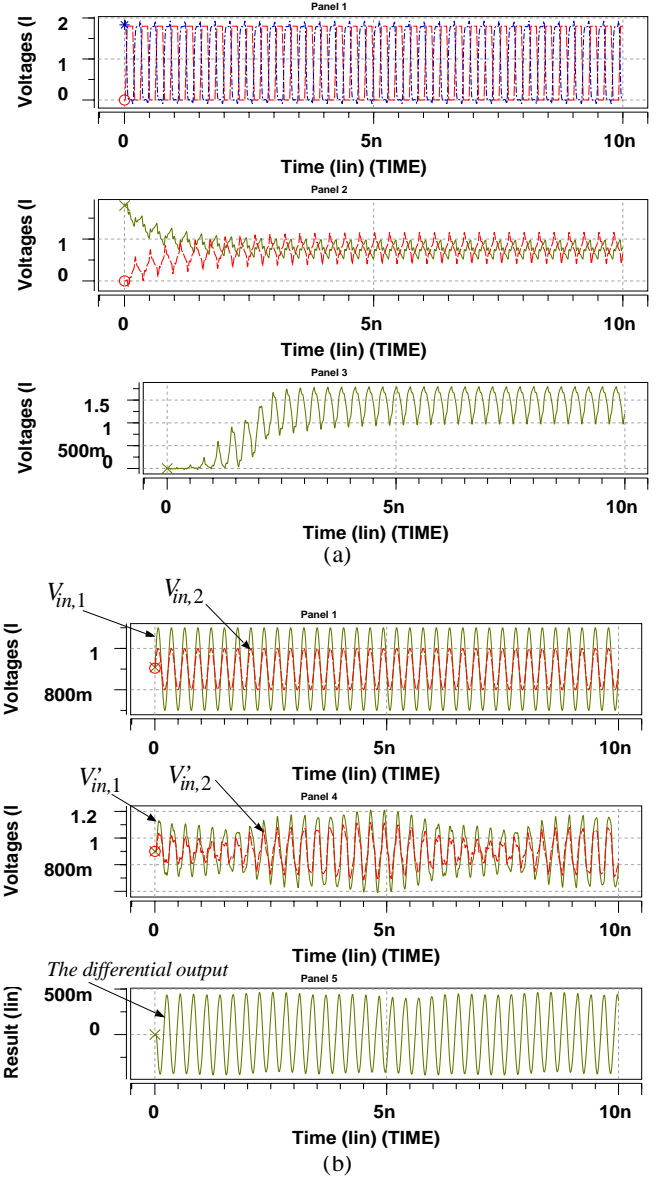


Fig. 8. (a) Input and output waveforms of Fig. 7 (a). (b) input and output signals of Fig. 7 (b).

The output voltage $V_{out,inv1}$ of the CMOS inverter in Fig. 8 (b) does not have a rail-to-rail swing because of the crosstalk noise effect from the other adjacent line. In fact, this CMOS inverter is incapable of generating a logic "LOW". On the other hand, the functionality of a CML buffer remains intact in the presence of the coupling noise from a neighboring line, as seen in Fig. 8 (b).

A CML buffer also shows a better performance in the presence of power/ground noise than a CMOS inverter. Noise on power and ground wires have very small degrading effects on the differential output voltage. Fig. 9 demonstrates a circuit that emulates the actual scenario where on-chip power/ground wires are modeled using distributed RC circuits; and the chip-package interface parasitics including parasitics associated with bondwires and package traces are modeled using (R_p, L_p, C_p) and (R_g, L_g, C_g) . A static CMOS inverter driving an off-chip load generates Power/ground fluctuations. Shown in figures 10 (a), (b), and (c) are the on-chip

power/ground waveforms, the single-ended outputs and the differential output of the CML buffer. The differential architecture is capable of filtering the common-mode noise and generates a clean differential output with a maximum of approximately 0.4V.

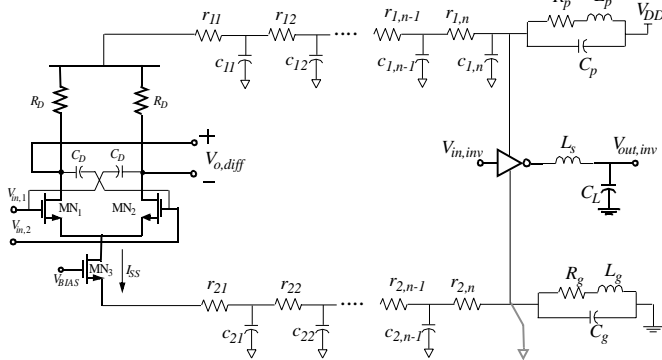


Fig. 9. CML buffer along with on-chip power/ground wires and chip-package interface circuit model.

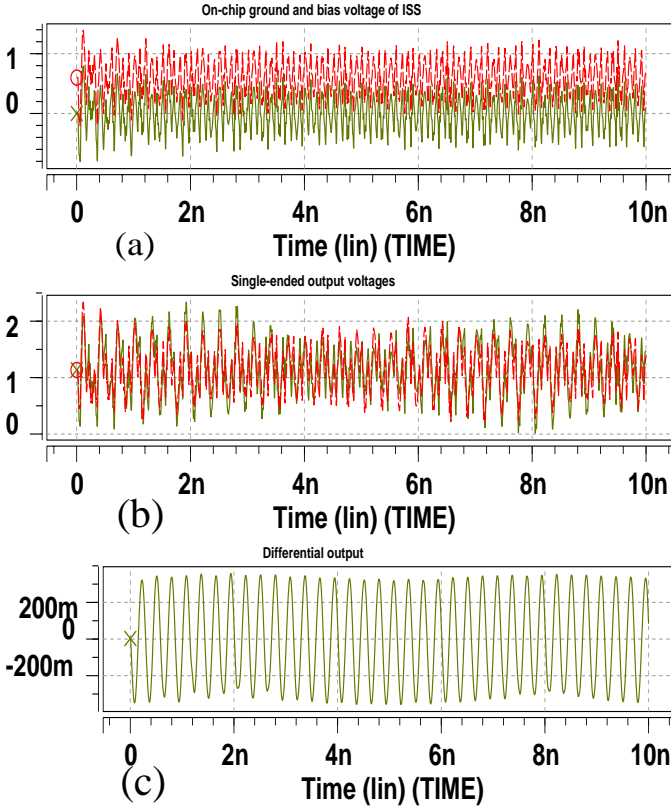


Fig. 10. (a) On-chip ground, input bias voltage of the tail current. (b) Single-ended output voltages of the CML buffer. (c) The differential output voltage of the CML buffer.

4.2. Tapered CML buffer experiment

Similar to a CMOS tapered buffer, a single CML buffer might not be sufficient to drive an off-chip load. There are, however, more design trade-offs involved in the design of a CML tapered buffer than in a CMOS tapered buffer. A superior high-frequency performance in a CML buffer is guaranteed only if the design guidelines explained thoroughly in Section 3 to be taken into consideration.

Fig. 11 (a) plots propagation delay as a function of number of CML stages for different values of X , where X is the ratio between the off-chip load impedance and the load impedance of the first pre-driver stage. In practice, X is between 30-100. The optimum number of buffer stages will thus be between 3-4. Fig. 11 (b) depicts the delay vs. number of stages for tapered CMOS buffer. The delay variation in terms of the number of stages for CML tapered buffer and CMOS tapered buffer are almost identical. However, the total propagation delay of a CML buffer chain for a given value of X is less than that of CMOS buffer chain, which is in accordance with what is expected. Remember that 50% propagation delay of a CMOS inverter is inversely proportional to NMOS and PMOS transconductance parameters and directly proportional to the load capacitance [1]. According to (11), the propagation delay of a CML buffer is directly proportional to the load capacitance (similar to a CMOS inverter) and the drain resistance. A larger threshold voltage and a lower drift velocity associated with a PMOS transistor cause the propagation delay of a CMOS inverter to be larger than that of a CML buffer that uses the same transistor size (Figures 11 (a) and (b)).

4.3. Inductive peaking

The inductive peaking was proposed as an efficient and simple circuit technique to speed up the buffer's response. Figures 12 (a) and (b) demonstrate the differential output voltage of a CML buffer without and with the inductive peaking, respectively. The inductance value is 4nH and signals are running at 5GHz which is the frequency set forth in SONER/SDH OC-48. The output voltages of CML buffer in the presence of inductance will have larger amplitude and as a result faster rise and fall times.

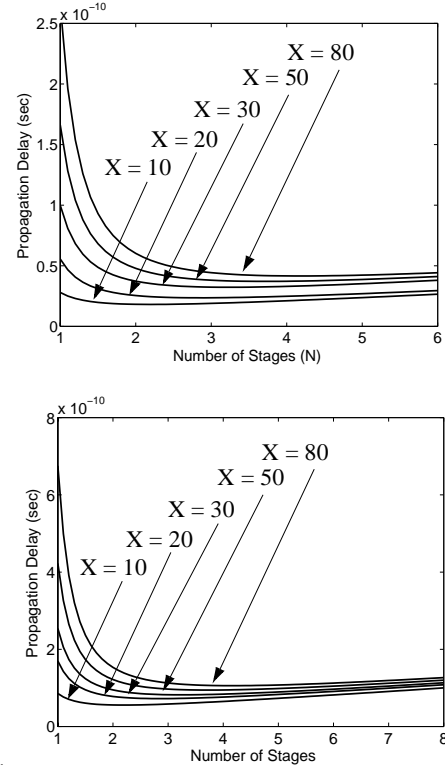


Fig. 11. (a) Delay vs. number of stages for CML tapered buffer chain. (b) Delay vs. number of stages for CMOS tapered buffer chain.

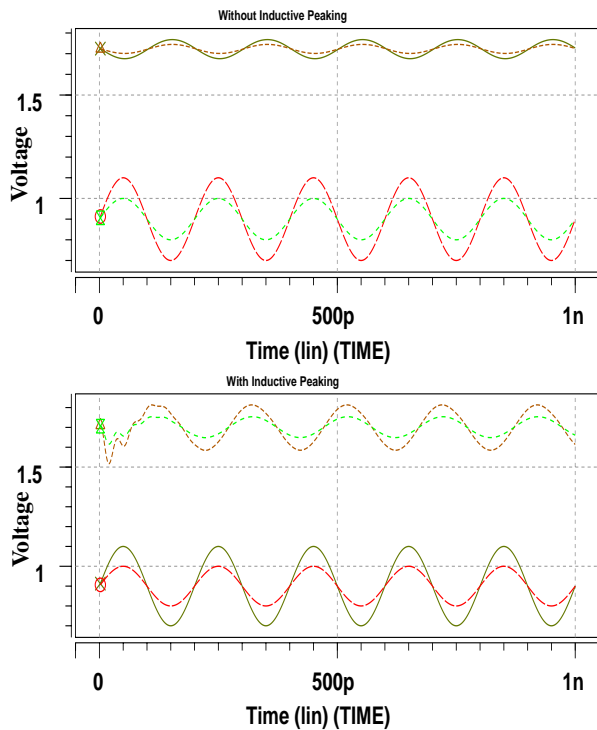


Fig. 12. (a) Input and output waveforms of a CML buffer without inductive peaking. (b) Input and output waveforms of a CML buffer with inductive peaking.

6. CONCLUSIONS

In this paper we investigated important problems involved in the design of a CML buffer as well as a chain of tapered CML buffers. A new design procedure to systematically design a chain of tapered CML buffers was proposed. We proved that the differential architecture of a CML buffer makes it functionally robust in the presence of environmental noise sources (e.g., crosstalk, power/ground noise). It was shown, both through the experiments and by using efficient analytical models, why CML buffers are better than CMOS inverters in high-speed low-voltage applications.

REFERENCES

- [1] J. Rabaey, *Digital Integrated Circuits: A Design Perspective*, Prentice-Hall, 1996.
- [2] B. Razavi, "Prospects of CMOS Technology for High-Speed Optical Communication Circuits," *IEEE J. Solid-State Circuits*, vol. 37, No. 9, pp. 1135-1145, Sept. 2002.
- [3] M. Mizuno, M. Yamashina, K. Furuta, H. Igura, H. Abiko, K. Okabe, A. Ono, H. Yamada, "A GHz MOS adaptive pipeline technique using MOS current-mode logic," *IEEE J. Solid-State Circuits*, vol. 31, No. 6, pp. 784-791, June 1996.
- [4] M. H. Anis, M. I. Elmasry, "Self-timed MOS current mode logic for digital applications," *IEEE Int'l Symp. on Circuits and Systems*, vol. 5, pp. 113-116, May 2002.
- [5] B. Razavi, *Design of Analog CMOS Integrated Circuits*, pp. 101-134, McGraw-Hill, 2001.
- [6] T. H. Lee, *The Design of CMOS Radio-Frequency Integrated Circuits*, Cambridge University Press, 1998.
- [7] N. Hedenstierna, K. O. Jeppson, "CMOS Circuit Speed and Buffer Optimization," *IEEE Trans. Computer-Aided Design*, vol. CAD-6, No. 2, pp. 270-281, March 1987.